Supplement of Atmos. Meas. Tech., 11, 6815–6832, 2018
https://doi.org/10.5194/amt-11-6815-2018-supplement

Atmospheric Measurement Techniques
Open Access
EGU

Supplement of

Low-pressure gas chromatography with chemical ionization mass spectrometry for quantification of multifunctional organic compounds in the atmosphere

Krystal T. Vasquez et al.

Correspondence to: Krystal T. Vasquez (kvasquez@caltech.edu) and Paul. O. Wennberg (wennberg@caltech.edu)

S1 Instrument Calibration

Instrument calibrations were performed using four authentic standards for hydrogen cyanide (HCN), sulfur dioxide (SO_2), hydroxyacetone (HAc) and glycolaldehyde (GLYC) with HRToF-CIMS. For HCN and SO_2, calibrations were performed using a standard gas mixture (300 ppmv in N_2 and 50 ppmv in N_2, respectively) which were individually diluted with N_2 using mass flow controllers prior to being sampled by the HRToF-CIMS. Cylinder concentrations of these two gases were verified using Fourier-transform infrared spectroscopy (FTIR) using cross section data archived in the Pacific Northwest National Lab (PNNL) IR database (Sharpe et al., 2004). Gas-phase HAc mixture was created by flowing dry N_2 over the commercially available compound (Aldrich, 90%) into a 0.1 m^3 bag made of fluorinated ethylene propylene (Teflon-FEP) to obtain several ppmv HAc. This mixture was then further diluted with N_2 after being measured by the FTIR before entering the instrument. Gas-phase GLYC was produced by flowing dry N_2 through a three-ported vial which contained the commercially available glycolaldehyde dimer (Aldrich). During this process, the three way vial was gently heated and cotton was inserted downstream of the vial to collect particles and low vapor pressure impurities before the gas was transferred to the 0.1 m^3 bag. The remainder of the procedure for GLYC mirrors that of HAc.

Though we were able to calibrate these four gases, many compounds of interest are not commercially available and difficult to synthesize and purify. Therefore, the above experiments were performed simultaneously on the cToF-CIMS in order to directly compare the sensitivities of these two instruments. On average, the cToF-CIMS was 1.37$\pm$0.22 times more sensitive than HRToF-CIMS under the same operating conditions of the field deployments. For the analysis described within the main text, we use this ratio between the two instrument sensitivities to convert previously determined cToF-CIMS sensitivities from calibrations or estimated from the ion-molecule collision rate which can be calculated using the dipole and polarizability of the analyte species (Paulot et al., 2009; Garden et al., 2009; Crounse et al., 2011).

S2 Instrument Characterization

A number of chamber experiments were performed to properly characterize the GC-HRToF-CIMS both prior to and following field deployment. A list of experiments discussed in this study can be found in Table S1.

S2.1 Reagents

1-propene (propene) (> 99%), 1-butene (> 99%), *cis*-2-butene (> 99%), *trans*-2-butene (> 99%) 2-methyl-propene (> 99%), isoprene (> 98%) and hydrogen peroxide (H_2O_2; 30% by weight in water) were purchased from Sigma Aldrich and used without further purification in the amounts listed in Table S1. A nitric oxide standard gas tank (NO; 1994 ppmv in high purity N_2) used for the majority of experiments was prepared by Matheson. Methyl nitrite (CH_3ONO) was synthesized, purified and stored in a glass trap submerged in liquid nitrogen using methods described in Taylor et al. (1980). In most cases, CH_3ONO served as the HO_x precursor.

S2.2 Chamber Experiments

Instrument characterization experiments were conducted in either a 0.1 m^3 or 0.8 m^3 Teflon bag with a 6.35 mm PFA port used for the introduction and sampling of gases. During each experiment, the bag was filled with appropriate concentrations of reactants and placed inside a enclosure with UV reflective surfaces and eight UV lights (λ_{peak} = 350 nm). Addition of the

alkene, CH_3ONO and NO was accomplished by filling a 500 cm^3 glass bulb with the compound to the desired pressure before filling with N_2 to reach approximately 993 hPa. If needed, the reagent gas was serially diluted up to two times by pumping down the bulb to the desired pressure and backfilling again with N_2. The contents of the bulb were then transferred to the chamber with the remaining bag volume filled with dry zero air. For experiment 4, H_2O_2 served as the HO_x source. Addition of H_2O_2 into the chamber was performed by flowing 20 L min^{-1} N_2 over 8 µL of H_2O_2 contained in a shallow glass vial for approximately 10 - 15 minutes to create a bag concentration of ~2 ppmv H_2O_2. In experiment 6, high RH conditions (~50%) were created by filling a portion of the bag volume with dry zero air that has passed through a water bubbler prior to entering the chamber.

Once all reagents were in the chamber bag, photochemistry was initiated upon illumination of 1-8 UV lights. Alkene oxidation occurred at approximately 298 K, with the exception of experiment 5 which was performed at an elevated temperature (315 K) to allow for increased rates of unimolecular isomerization. Experiment 5 also required longer peroxy radical lifetimes to produce a sufficient GC signal of these isomerization products. This was performed by using a single UV light in which all direct radiation was blocked allowing only the photons scattered off the walls to contribute to the chemistry.

For the majority of experiments, photochemistry was stopped when approximately 10% of the alkene had reacted, to minimize secondary chemistry of products. Chamber air was then sampled by the GC-HRToF-CIMS at approximately 2-3 L min^{-1} through ~2.4 m of 5.84 mm ID tubing to reduce residence time in and speed equilibration of the sampling line. Chamber analysis typically alternated between the direct CIMS and GC-CIMS sampling to assess any changes in concentration or transmission that may occur throughout the experiment. In most cases, GC effluent was directed into the ion source to allow for enhanced signal to noise (IS mode, see main text). Divergence from this procedure occurred during experiments 1 and 2 when determining the ion source enhancement ratio. During this time, each GC cycle alternated between IS mode and FT mode and the ratio of these two types of GC signals which were used to determine the signal enhancement. A similar procedure was followed when assessing the GC transmission of targeted analytes. In addition, output from the GC during trapping was also occasionally directed into the mass spectrometer to monitor potential breakthrough.

Table S1. Instrument characterization experiment list

Expt	HO_x Source, ppbv	NO, ppbv	VOC, ppbv	Objective
1	CH_3ONO, 50	100	Isoprene, 50	IonSrc Enhancement Ratio
2	CH_3ONO, 100	500	Isoprene, 100	IHN Transmission IonSrc Enhancement Ratio
3	CH_3ONO, 100	500	Isoprene, 100	IHN Peak Assignment
4	H_2O_2, 2000	0	Isoprene, 100	ISOPOOH + IEPOX Peak Assignment ISOPOOH + IEPOX Transmission
5	CH_3ONO, 100	0	Isoprene, 100	HPALD Peak Assignment
6	CH_3ONO, 100	500	Isoprene, 100	Column Humidity Effect
7	CH_3ONO, 100	500	*trans*-2-Butene, 100	Butene HN Peak Assignment
8	CH_3ONO, 100	500	2-methyl-Propene, 100	Butene HN Peak Assignment
9	CH_3ONO, 100	500	1-Butene, 100	Butene HN Peak Assignment
10	CH_3ONO, 100	500	*cis*-2-Butene, 100	Butene HN Peak Assignment
11	CH_3ONO, 100	500	Propene, 100	Propene HN Peak Assignment
12	CH_3ONO, 100	500	Propene, 100 Isoprene, 100	Trap Linearity Test

S3 Previous Design of GC Assembly

Instrument upgrades occurred between the PROPHET and Caltech field studies to improve the chromatography and significantly reduce the need for GC downtime due to cooling system maintenance. These upgrades included a redesign of the GC assembly, which was necessary to fix some key issues experienced at PROPHET, such as large temperature gradients across the column and poor temperature control as a whole. The previous version of the field deployable GC assembly can be seen in Fig. S1. Rather than two aluminum plates, this assembly consisted of a thin copper band. The column rested along the inner diameter of this band and was held within a 1.59 mm O.D. copper tube. The GC was cooled as liquid $\mathrm{CO_2}$ expanded and flowed along 3.18 mm tubing that was soldered onto the inside of the band (to increase thermal contact). The $\mathrm{CO_2}$ liquid entered at one location in the ring positioned near the two ends of the column and its flow was split at a stainless steel tee to allow both sides of the ring to cool evenly. $\mathrm{CO_2}$ flow and temperature were regulated as described in the main text, however GC temperature was measured at only one location on the ring, near the $\mathrm{CO_2}$ inlet (Fig. S1, red star).

Unfortunately, by having the $\mathrm{CO_2}$ flow enter through only one location in the ring, we found that the temperature gradient of opposite sides of the ring could exceed several degrees. In addition, because temperature was only monitored in one location near the coldest point of the column, it is difficult to assess the quality of the GC trapping conditions. In contrast, the redesigned GC allows $\mathrm{CO_2}$ to enter from the center of the plates and move outward to the diameter of the column ring. This ensures that the entire GC column is cooled at approximately the same rate. Furthermore, the addition of two more RTDs along the column also allow us to monitor the temperature gradient in real time and provides finer temperature control overall.

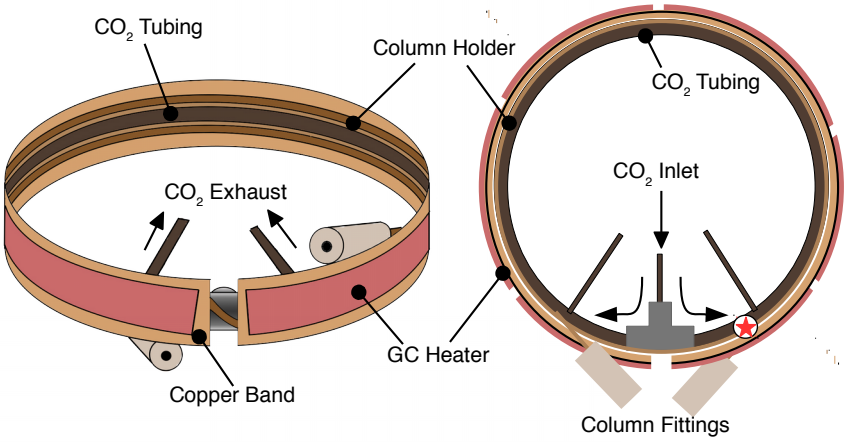

Figure S1. Original design of the GC cryotrapping and heating assembly used during the PROPHET campaign. Here, the GC assembly consists of a thin copper band. The GC column is held within a 1.59 mm O.D. copper tube which makes thermal contact along the inner diameter of the outer band. To cool the column, the $\mathrm{CO_2}$ enters through a short pieces of 3.18 mm O.D. copper tubing and its flow is split at a stainless steel tee (as shown in the right diagram) so both sides of the ring can cool evenly. Heaters are adhered to the outside of the copper band (red) and GC temperature was monitored at one location, marked by a red star.

S4 GC Cryotrap Performance

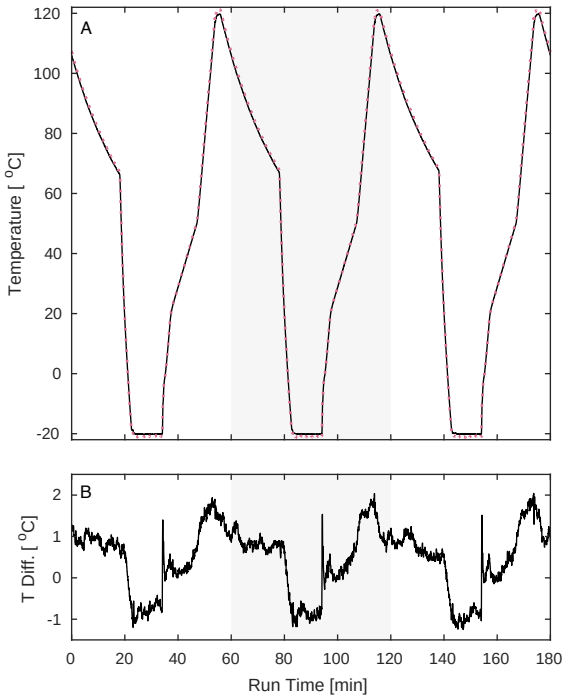

Figure S2. (A) Temperature profiles for three consecutive GC runs demonstrating the reproducibility of GC temperature despite frequent thermal cycling. (B) Temperature difference between locations (1) and (2) on the GC (see Fig. 2, main text) show a consistently small temperature gradient ($< 2^{o}$C) across the column during the temperature program. Ambient temperatures during these GC cycles ranged between 27.8 - 33.2^{o}C.

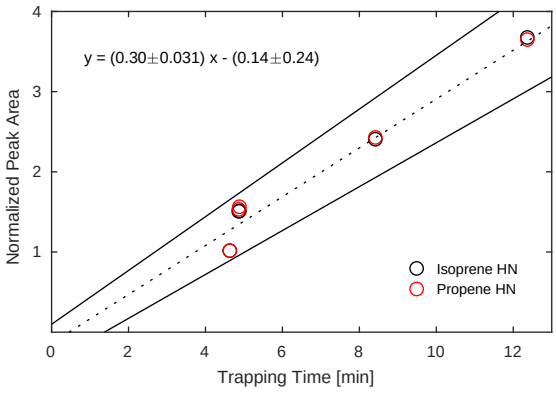

Figure S3. Chromatogram peak areas as a function of trapping time (and, as a result, trapping volume). Analytes were cryofocused on the GC column held at -20°C. Circles represent the sum of the peak areas of the two dominant IHN isomers (black) and the two isomers of propene HN (red) normalized to samples trapped at 4 minutes.

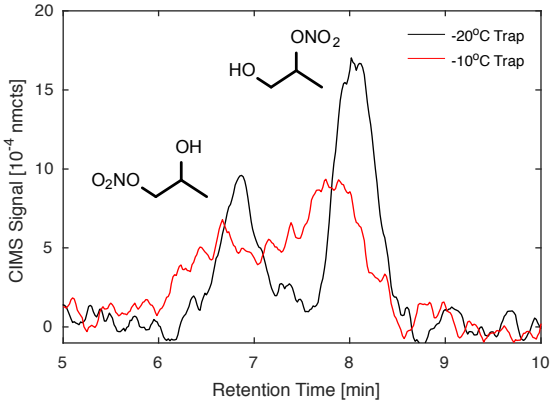

Figure S4. Comparison of consecutive chromatograms obtained during the Caltech field study of propene HN trapped at -20°C (black) and -10°C (red), demonstrating the effect trapping temperature can have on the chromatography of higher volatile species.

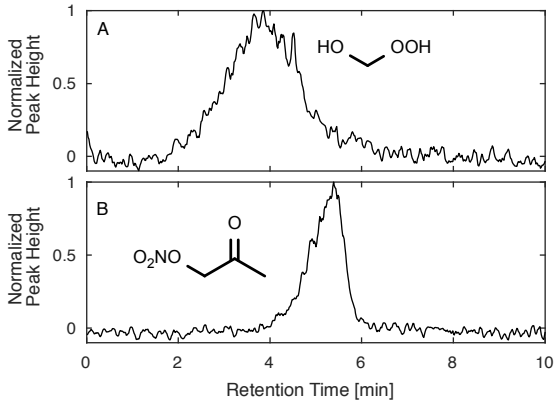

Figure S5. Chromatograms obtained during the Caltech field study field data for (A) hydroxymethyl hydroperoxide (HMHP) and (B) propanone nitrate (PROPNN) demonstrating irregular peak shapes that can result for higher volatility species during typical trapping conditions used in this study. Further optimization of GC cryotrapping is needed in order to better quantify these compounds through GC analysis. GC signal shown here has been normalize to the largest peak in the displayed window.

S5 Ion Fragmentation

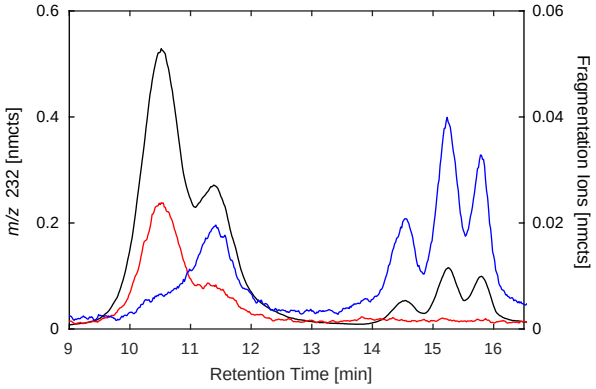

Figure S6. Examples of fragmentation ions of IHN resulting from direct electron attachment to IHN. The primary product ion from IHN clustering with CF_3O^- (*m/z* 232, black) is compared with fragmentation ions resulting from electron attachment (*m/z* 99, blue and *m/z* 146, red) These fragment ions can provide additional structural information. For example *m/z* 99 has high yields from primary and secondary IHN structures while *m/z* 146 has high yields from β-hydroxy nitrates.

References

Crounse, J. D., Paulot, F., Kjaergaard, H. G., and Wennberg, P. O.: Peroxy radical isomerization in the oxidation of isoprene, Phys Chem Chem Phys, 13, 13 607 – 13 613, https://doi.org/10.1039/C1CP21330J, 2011.

Garden, A. L., Paulot, F., Crounse, J. D., Maxwell-Cameron, I. J., Wennberg, P. O., and Kjaergaard, H. G.: Calculation of conformationally weighted dipole moments useful in ion–molecule collision rate estimates, Chem Phys Lett, 474, 45–50, https://doi.org/10.1016/j.cplett.2009.04.038, 2009.

Paulot, F., Crounse, J. D., Kjaergaard, H. G., Kroll, J. H., Seinfeld, J. H., and Wennberg, P. O.: Isoprene photooxidation: new insights into the production of acids and organic nitrates, Atmos Chem Phys, 9, 1479 – 1501, https://doi.org/10.5194/acp-9-1479-2009, 2009.

Sharpe, S. W., Johnson, T. J., Sams, R. L., Chu, P. M., Rhoderick, G. C., and Johnson, P. A.: Gas-Phase Databases for Quantitative Infrared Spectroscopy, Appl Spectrosc, 58, 1452–1461, https://doi.org/10.1366/0003702042641281, https://doi.org/10.1366/0003702042641281, pMID: 15606959, 2004.

Taylor, W. D., Allston, T. D., Moscato, M. J., Fazekas, G. B., Kozlowski, R., and Takacs, G. A.: Atmospheric photodissociation lifetimes for nitromethane, methyl nitrite, and methyl nitrate, Int J Chem Kinet, 12, 231 – 240, https://doi.org/10.1002/kin.550120404, 1980.